



Published in final edited form as:

*Pediatr Res.* 2021 February ; 89(3): 456–463. doi:10.1038/s41390-020-1064-6.

## The Newborn *Fmr1* Knockout Mouse: A Novel Model of Excess Ubiquinone and Closed Mitochondrial Permeability Transition Pore in the Developing Heart

Matthew Barajas<sup>1</sup>, Aili Wang<sup>1</sup>, Keren K. Griffiths<sup>1</sup>, Kenji Matsumoto<sup>2</sup>, Rui Liu<sup>2</sup>, Shunichi Homma<sup>2</sup>, Richard J. Levy<sup>1,\*</sup>

<sup>1</sup>Department of Anesthesiology, Columbia University Medical Center, New York, NY

<sup>2</sup>Department of Medicine, Columbia University Medical Center, New York, NY

### Abstract

**Background:** Mitochondrial permeability transition pore (mPTP) closure triggers cardiomyocyte differentiation during development while pathological opening causes cell death during myocardial ischemia-reperfusion and heart failure. Ubiquinone modulates the mPTP, however, little is known about its mechanistic role in health and disease. We previously found excessive proton leak in newborn *Fmr1* KO mouse forebrain caused by ubiquinone deficiency and increased open mPTP probability. Because of the physiological differences between the heart and brain during maturation, we hypothesized that developing *Fmr1* KO cardiomyocyte mitochondria would demonstrate dissimilar features.

**Methods:** Newborn male *Fmr1* KO mice and controls were assessed. Respiratory chain enzyme activity, ubiquinone content, proton leak, and oxygen consumption were measured in cardiomyocyte mitochondria. Cardiac function was evaluated via echocardiography.

**Results:** In contrast to controls, *Fmr1* KO cardiomyocyte mitochondria demonstrated increased ubiquinone content and decreased proton leak. Leak was cyclosporine (CsA)-sensitive in controls and CsA-insensitive in *Fmr1* KOs. There was no difference in absolute mitochondrial respiration or cardiac function between strains.

---

Users may view, print, copy, and download text and data-mine the content in such documents, for the purposes of academic research, subject always to the full Conditions of use:[http://www.nature.com/authors/editorial\\_policies/license.html#terms](http://www.nature.com/authors/editorial_policies/license.html#terms)

\*Correspondence: Richard J. Levy, MD, FAAP, Department of Anesthesiology, 622 W. 168<sup>th</sup> Street, PH5-534B, New York, NY 10032, 212-305-3884, RL2740@cumc.columbia.edu.

Author contributions:

- Substantial contributions to conception and design, acquisition of data, or analysis and interpretation of data: MB, AW, KG, KM, RL, SH, RJL
- Drafting the article or revising it critically for important intellectual content: MB, KM, RL, SH, RJL
- Final approval of the version to be published: MB, AW, KG, KM, RL, SH, RJL

Disclosure statement: The authors declare no competing interests

Patient consent was not required

Category of study: Basic Science

**Conclusion:** These findings establish the newborn *Fmr1* KO mouse as a novel model of excess ubiquinone and closed mPTP in the developing heart. Such a model may help provide insight into the biology of cardiac development and pathophysiology of neonatal heart failure.

## Introduction

Heart failure in the newborn is a challenging clinical condition that results from a variety of congenital and acquired conditions (1, 2). Cardiac dysfunction can manifest from structural abnormalities or ischemia-reperfusion injury related to surgery in children with congenital heart disease and can develop as a consequence of primary cardiomyopathies in infants with a structurally normal heart (1–3). Unfortunately, therapy for neonatal heart failure remains nonspecific due to a lack of mechanistic insight and incomplete understanding of normal cardiomyocyte development (1, 2).

Recent investigation has helped to elucidate the role of mitochondria in the developing heart (2). In embryonic cardiomyocytes, the respiratory chain is immature and bioenergetic capacity is generated primarily via anaerobic glycolysis (4, 5). As the heart matures, the mitochondrial membrane potential is established and oxidative phosphorylation becomes the predominant source of cellular energy (2, 4). This change, mediated by closure of the mitochondrial permeability transition pore (mPTP), reduces oxidative stress and triggers cardiomyocyte differentiation (6). Murine cardiac mitochondria are relatively immature at birth, but undergo maturation in the first 2 weeks of life (2). However, the probability of mPTP opening remains high in postnatal cardiomyocyte mitochondria, rendering the neonatal heart vulnerable to injury (2).

High-conductance opening of the mPTP collapses the mitochondrial membrane potential, uncouples oxidative phosphorylation, results in mitochondrial swelling, and leads to apoptosis or necrosis (4, 7, 8). Pathological mPTP opening is thought to play a role in myocardial ischemia-reperfusion injury and heart failure (4, 9, 10). A number of agents, such as cyclosporine A (CsA), are known to target and inhibit the mPTP and have been shown to protect the heart in preclinical models (10, 11). However, such approaches have failed to translate to the clinical scenario and, currently, mitochondrial therapy for neonatal heart failure is limited to nonspecific agents such as carnitine and coenzyme Q (CoQ)(12–14).

CoQ, or ubiquinone, is a lipophilic mobile electron carrier within the respiratory chain (15). In addition, CoQ<sub>10</sub> and other ubiquinone analogues have been shown to have biological activity on the mPTP, modulating channel opening by inhibition or activation (16). In a handful of clinical trials, CoQ supplementation was shown to be safe and effective in adult heart failure patients, improving cardiac function and short-term survival while reducing major adverse cardiovascular events (17, 18). However, mechanistic data is lacking and CoQ therapy for cardiomyopathy in children has been poorly studied (19). Thus, there is need to investigate the biological effects of CoQ on pathological opening of the mPTP in the developing heart. In order to do so, as a first step, novel and relevant preclinical models need to be identified and established.

Interestingly, the physiological role of the mPTP in developing cardiomyocytes differs from that of immature neurons (4). In contrast to cardiac mitochondria, inhibition and closure of the pore in neural progenitors enhances proliferation while prolonged mPTP opening promotes neuronal differentiation (4, 20). We previously found excessive proton leak in forebrain mitochondria in a newborn mouse model of Fragile X syndrome (*Fmr1* knockout) caused by CoQ deficiency and an open CsA-sensitive channel (the mPTP) (21). Fragile X syndrome (FXS) is caused by silencing of the *Fmr1* gene and loss of expression of the gene product, fragile X mental retardation protein (FMRP) (22). FMRP is a translational repressor that binds to the mRNA of all of the known enzymes of the ubiquinone biosynthesis pathway, however, it is unknown how loss of FMRP causes changes in CoQ levels (23). Because of the physiological differences between the immature heart and brain, we hypothesized that developing *Fmr1* KO cardiomyocyte mitochondria would demonstrate dissimilar features from immature neurons. In stark contrast to the *Fmr1* KO forebrain and the immature wild-type heart, we found increased levels of ubiquinone, decreased proton leak, and closed probability of the mPTP in newborn *Fmr1* KO cardiomyocyte mitochondria. The importance of these findings is that it establishes a model of excess CoQ and a closed pore in the developing heart. Such a model will be a valuable tool in the quest to better understand the role of ubiquinone and the mPTP in neonatal heart failure in future work.

## Methods

### Animals

The care of the animals in this study was in accordance with NIH and Columbia University Medical Center Institutional Animal Care and Use Committee guidelines and conformed to the provisions of the Animal Welfare Act (NIH/DHHS) and the Association for Assessment and Accreditation of Laboratory Animal Care (AAALAC). Six to eight week old hemizygous male (*Fmr1*<sup>-Y</sup>) (FVB.129P2-Pde6b<sup>+</sup> Tyr<sup>c-ch</sup> Fmr1<sup>tm1Cgr/J</sup>) and homozygous female (*Fmr1*<sup>-/-</sup>) mice were acquired (Jackson Laboratory, Bar Harbor, ME), paired, and mated to yield *Fmr1* KO neonatal male pups. Control (FVB.129P2-Pde6b<sup>+</sup> Tyr<sup>c-ch</sup>/AntJ) hemizygous male and homozygous female breeding pairs were also acquired (Jackson Laboratory, Bar Harbor, ME) and mated to yield pups that expressed wild-type FMRP. Experiments were performed on 10 day old male pups given the male predominance in Fragile X syndrome. For FMRP expression, FVB male pups were evaluated on P7 and P10.

### Immunoblot analysis

10µg samples of forebrain and cardiac ventricular homogenate were subjected to SDS-acrylamide gel electrophoresis and immunoblotting. FMRP expression was assessed using a primary polyclonal rabbit anti-FMRP antibody (Abcam ab17722). Cytosolic protein loading was assessed with a primary monoclonal antibody to mouse  $\alpha$ -tubulin (Millipore Sigma T5168). Appropriate secondary antibodies were utilized, signal was detected with enhanced chemiluminescence (ECL; Amersham Pharmacia Biotech, Piscataway, New Jersey, USA), and density was measured using scanning densitometry. FMRP density was normalized to tubulin and FVB P7 heart values were arbitrarily set to equal 1.

### Mitochondrial isolation

Cardiac ventricles were harvested and homogenized in ice-cold isolation buffer (225 mM mannitol, 75 mM sucrose, 1 mM EGTA, 5 mM HEPES-KOH (pH 7.2) and 1 mg/mL of fatty-acid-free bovine serum albumin (BSA)). The homogenate was spun at 1100 *g* for 5 min at 4 °C. Supernatant (0.8 mL) was removed and centrifuged at 18,500 *g* for 10 min at 4 °C 15 vol% Percoll gradient. The mitochondria fraction was collected and resuspended in 1 mL of washing buffer (250 mM sucrose, 5 mM HEPES-KOH (pH 7.2), 1 mM EGTA and 1 mg/mL of BSA). The suspension was centrifuged at 10,000 *g* for 10 min at 4 °C. The mitochondrial pellet was resuspended in 0.035 mL of washing buffer and mitochondrial protein concentrations were determined using the method of Lowry.

### Steady-state electron transport chain enzyme activity

Respiratory chain enzyme complex activities were measured spectrophotometrically as previously described in 1-mL volume (24, 25). Rotenone-sensitive Complex I specific activity was measured in isolated mitochondria (40 µg) using 4.8 mM<sup>-1</sup> cm<sup>-1</sup> as the extinction coefficient of NADH at 340 nm with the reference wavelength of 380 nm. TTFA (2-thenoyltrifluoroacetone)-sensitive Complex II activity was determined in isolated mitochondria (40 µg) using 19.1 mM<sup>-1</sup> cm<sup>-1</sup> as the extinction coefficient of 2,6-dichlorophenolindophenol (DCPIP) at 600 nm. For Complex III, antimycin A-sensitive first-order rate constants were calculated in isolated mitochondria (4 µg) using 18.5 mM<sup>-1</sup> cm<sup>-1</sup> as the extinction coefficient of cytochrome *c* at 550 nm. Rotenone-sensitive Complex I+III linked activity and antimycin A-sensitive Complex II+III linked activity were determined separately in isolated mitochondria (40 µg) using 18.5 mM<sup>-1</sup> cm<sup>-1</sup> as the extinction coefficient of cytochrome *c* at 550 nm.

### Ubiquinone quantification

Ubiquinone was extracted from isolated cardiomyocyte mitochondria (1.5–3 mg) using Tween-20 (3%), cold (–20°C) methanol (300 µL), and light petroleum (450 µL) (26, 27). Samples were centrifuged at 2200 *g* for 15 minutes at room temperature. Supernatant was collected, evaporated in a glass tube, and resuspended in 100% ethanol. Total ubiquinone was calculated in 400 µL from the difference in spectra (oxidized minus sodium borohydride reduced) using an absorption coefficient of 12.25 mM<sup>-1</sup> cm<sup>-1</sup> at 275 nm (27).

### Proton leak kinetics

Proton leak relative to the proton motive force was measured as previously described (28). Oxygen consumption and mitochondrial membrane potential were measured simultaneously using ventricular cardiomyocyte mitochondria (0.1 mg) in 1-mL of respiration buffer (200 mM sucrose, 25 mM KCl, 2 mM K<sub>2</sub>HPO<sub>4</sub>, 5 mM HEPES-KOH (pH 7.2), 5 mM MgCl<sub>2</sub>, 0.2 mg/mL BSA) containing 80 ng/mL nigericin (to collapse  $\Delta\psi$ ) and 5 µM rotenone at 37°C. Membrane potential was determined using an ion sensitive electrode selective for the lipophilic cation, tetraphenylphosphonium (TPP<sup>+</sup>) (World Precision Instruments, Sarasota, FL), and calculated using the Nernst equation as previously described (29). Mitochondrial respiration was initiated with 5 mM succinate. State 4 was induced with oligomycin (2.5 µg/mL) and respiration was titrated with malonate (up to 2 mM). In separate experiments,

titrations of malonate (0.1 mM) were used to induce voltage-gated proton leak during state 4 respiration and cyclosporine A (CsA, 1  $\mu$ M), carboxyatractyloside (cAT, 1  $\mu$ M), and guanosine diphosphate (GDP, 0.75 mM) were added to specifically inhibit the mPTP, the adenine nucleotide translocase (ANT), and uncoupling proteins (UCPs), respectively to determine source of leak (30, 31). cAT was added after CsA given the potential to open the mPTP. The effect of the CsA solvent, ethanol, was tested independently. The ubiquinone analog, decylubiquinone (DUB, 100  $\mu$ M), was used in separate experiments to antagonize endogenous CoQ (21).

### Mitochondrial oxygen consumption

Ventricular cardiomyocyte mitochondria (50  $\mu$ g) were added to 0.5 mL of respiration buffer (200 mM sucrose, 25 mM KCl, 2 mM K<sub>2</sub>HPO<sub>4</sub>, 5 mM HEPES-KOH (pH 7.2), 5 mM MgCl<sub>2</sub>, 0.2 mg/mL BSA). Oxygen consumption was measured using a Clark-type electrode (Oxytherm, Hansatech, UK) with Complex I-dependent substrates (10 mM glutamate and 5 mM malate) or Complex II-dependent substrate (10 mM succinate in the presence of 5  $\mu$ M rotenone) at 32°C. State 2 respiration was determined following the addition of substrates and ADP (200  $\mu$ M) was added to initiate state 3 respiration. The respiratory control ratio (RCR) was calculated as state 3 respiration divided by the state 4 rate observed following ADP consumption. The ADP-to-oxygen ratio (ADP:O) was calculated from the amount of ADP and oxygen consumed during state 3 respiration. Separately, state 4 respiration was induced with oligomycin (2.5  $\mu$ g/mL) and uncoupled state 3 respiration was induced with dinitrophenol (DNP) (70  $\mu$ M).

### Echocardiography

Transthoracic echocardiographic measurement of left ventricular cardiac function was performed as previously described (32). Mice were lightly sedated with i.p. ketamine (12.5 mg/kg) and xylazine (2 mg/kg) and then subjected to two-dimensional echocardiography using a Vevo770 High-Resolution Imaging System (VisualSonics, Inc., Toronto, Canada) with a 55-MHz transducer (RMV708, VisualSonics, Inc., Toronto, Canada). M-mode images and two-dimensional parasternal short axis images at the midpapillary level were obtained and recorded in a digital format by an investigator blinded to mouse genotype (K.M.). Images were then analyzed offline in a blinded manner (K.M.). Heart rate, end-diastolic left ventricular dimension, and end-systolic left ventricular dimension were measured. The percent fractional shortening was then calculated.

### Statistical analysis

Statistical analysis was performed using GraphPad Prism 8 software (GraphPad Software, La Jolla, CA). Data was assessed for normality by examining histograms and box plots and are presented as means  $\pm$  SD. The sample number of animals studied for each experiment is indicated in each figure. Differences between the two strains were assessed using a two-tailed, unpaired Student t test. Significance was set at  $P < 0.05$ .

## Results

### Fragile X Mental Retardation Protein (FMRP) is Expressed in the Developing Heart.

FXS is caused by genetic silencing of the *Fmr1* gene and loss of the gene product, FMRP (22). Although predominantly expressed within the brain and testis, FMRP is ubiquitous (33). However, little is known about FMRP expression in the developing heart. So, we first assessed for wild-type FMRP expression within the immature ventricular myocardium of FVB controls in the first two weeks of life (Figure 1). Using immunoblot analysis, we detected myocardial FMRP expression at 7 and 10 days of life in healthy controls (Figure 1). Thus, FMRP is expressed in the wild-type developing heart. Based on these findings, we performed our analyses on P10 given that, in the mouse, this age is analogous to a postnatal time point in human infancy (34).

### Ubiquinone is Increased in *Fmr1* KO Myocardium

Given our findings in the developing *Fmr1* KO forebrain we next measured CoQ levels in cardiomyocyte mitochondria of *Fmr1* KO mice and FVB controls on P10. CoQ is best known as a carrier of electrons from Complexes I and II to Complex III within the respiratory chain (15). So, we first measured the kinetic activity of Complexes I, II, and III, individually, and then determined the linked kinetic activities of Complex I+III and Complex II+III to indirectly quantify the CoQ pool. There were no significant differences in the kinetic activities of Complex I, II, or III between strains (Figure 2). However, the linked activities of both Complex I+III and Complex II+III were significantly increased in cardiomyocyte mitochondria from *Fmr1* KO mice compared to controls, suggesting CoQ excess (Figure 2). We confirmed these findings by directly quantifying mitochondrial ubiquinone content via spectrophotometry and found significantly increased levels of myocardial CoQ in *Fmr1* KOs versus controls (Figure 2). Thus, ubiquinone was increased in the developing *Fmr1* KO heart.

### *Fmr1* KO Mitochondria Demonstrate Less Proton Leak than Controls

Because the mPTP is a source of uncoupled hydrogen ion conductance and can be modulated by ubiquinone and its analogues, we next assessed proton leak in cardiomyocyte mitochondria of *Fmr1* KO mice and FVB controls on P10 (16, 35). To do so, we measured proton conductance relative to the proton motive force (36). The benefit of this approach is that it permits dynamic measurement of respiration over a range of mitochondrial membrane potentials. To assess proton leak kinetics, succinate-dependent respiration was initiated in state 4 using oligomycin and was titrated with serial additions of malonate (36). Using this approach, we found the *Fmr1* KO conductance curve to be right-shifted relative to FVB controls suggesting less proton leak (Figure 3a). In support of this, the rate of mitochondrial respiration was significantly lower in *Fmr1* mutants at the highest common membrane potential confirming less leak and more efficient respiration (Figure 3a).

Because proton leak can also be mediated by the adenine nucleotide translocase (ANT) and uncoupling proteins (UCPs), we next utilized specific inhibitors to delineate the source(s) of leak in each group (30, 31). Succinate-dependent state 4 respiration was initiated with oligomycin in freshly isolated cardiomyocyte mitochondria and malonate was added to

reduce the membrane potential and unmask any voltage-gate leak. CsA, carboxyatractyloside (cAT), and guanosine diphosphate (GDP) were subsequently added to inhibit the mPTP, the ANT, and UCPs, respectively (Figure 3b). In control mitochondria, CsA increased and stabilized the membrane potential and simultaneously reduced the oxygen consumption rate, indicating increased open probability of the mPTP (Figure 3b). The respiration rate declined further after addition of cAT, suggesting the ANT as an additional source of leak in control mitochondria (Figure 3b). In contrast, CsA failed to decrease oxygen consumption or increase membrane potential in *Fmr1* KO mitochondria, indicating closed probability of the mPTP (Figure 3b). Instead, respiration increased and membrane potential declined following the addition of CsA in *Fmr1* KOs, likely due to the uncoupling effect of the ethanol solvent in the absence biological activity of CsA on the mPTP (37). This ethanol-mediated effect was confirmed in mitochondria from both strains during state 4 respiration (Figure 3c). With regard to other sources of leak, respiration rates decreased after the addition of cAT and the membrane potential began to stabilize, suggesting the ANT as a source of proton leak in *Fmr1* KOs (Figure 3b). Lack of GDP sensitivity in both strains ruled out UCPs as a source of leak in *Fmr1* KOs or controls (Figure 3b).

We then tested the hypothesis that the CoQ-antagonizing quinone, decylubiquinone (DUB), would open the pore in both strains (i.e., antagonize endogenous CoQ in controls and excess CoQ in *Fmr1* KOs). Succinate-dependent state 4 respiration was initiated with oligomycin in freshly isolated cardiomyocyte mitochondria and DUB was added. DUB caused an immediate increase in respiration and concomitant decline in membrane potential, suggesting opening of a leak channel in both groups (Figure 3d). Importantly, both the increase in respiration and the fall in membrane potential following the addition of DUB were significantly greater in *Fmr1* KOs versus controls (Figure 3d). CsA increased the membrane potential and simultaneously reduced the oxygen consumption rate in both strains, indicating DUB-mediated opening of the mPTP (Figure 3d). Taken together, the data indicate open probability of the mPTP in the wild-type heart on P10 and excess ubiquinone and closed mPTP probability in developing *Fmr1* KO myocardium. The DUB-mediated effect in *Fmr1* KOs suggested a link between increased CoQ levels and the closed pore in *Fmr1* KO cardiomyocyte mitochondria.

### Mitochondrial Oxygen Consumption is Unaffected in *Fmr1* KO Cardiomyocytes

In order to understand the effect of increased levels of CoQ and closed probability of the mPTP on bioenergetic capacity, we next measured oxygen consumption using a Clark-type electrode in freshly isolated cardiomyocyte mitochondria from P10 *Fmr1* KOs and FVB controls. We quantified the rates of mitochondrial respiration for both Complex I-and Complex II-dependent substrates (Figure 4). There were no significant differences between strains regardless of substrate (Figure 4). Thus, excess ubiquinone and closed probability of the mPTP in the developing *Fmr1* KO heart did not affect absolute mitochondrial respiration.

### Cardiac Function is Unaffected in Newborn *Fmr1* KO mice

Prior work revealed evidence of open probability in the developing postnatal murine heart and that inhibition of the mPTP enhanced murine cardiac function in the neonatal period (2). Therefore, we assessed cardiac performance in *Fmr1* KO mice and FVB controls on P10 using two-dimensional transthoracic echocardiography. There were no differences in heart rate, left ventricular end-diastolic dimension, left ventricular end-systolic dimension, or fractional shortening between strains (Table, Figure 5). Thus, increased CoQ levels and closed probability of the mPTP in the *Fmr1* KO heart did not translate into an effect on cardiac function in newborn mutants.

### Discussion

The mPTP has been shown to have a high probability of opening in the neonatal murine heart (2). Consistent with this, we found evidence of open probability of the mPTP in wild-type cardiomyocyte mitochondria on P10. Although the regulatory factors involved in closing the mPTP in immature mitochondria during development are unknown, endogenous molecules, such as ubiquinone, have been shown to be capable of modulating the pore (16). Levels of CoQ are relatively low in infancy, peak in young adulthood, and decline thereafter (38). Thus, it is possible that temporal differences in biosynthesis of CoQ contribute to the high probability of mPTP opening in the immature heart. In contrast to wild-type controls, we identified relatively increased levels of ubiquinone, decreased proton leak, and closed probability of the mPTP in developing cardiomyocyte mitochondria of *Fmr1* KO mice on P10. These findings establish the newborn *Fmr1* KO mouse as a novel model of excess CoQ and a closed pore in the developing heart. Because it is unknown how quinones inhibit or activate the pore, such a model will serve as an important tool to help us better understand the biological interaction between CoQ and the mPTP in the immature heart during health and disease (16).

CoQ deficiency can cause heart failure and can result from it (39, 40). Lower myocardial ubiquinone levels have been associated with more severe heart failure symptoms and worse cardiac function in humans (39). In a small number of contemporary clinical trials in adults, CoQ<sub>10</sub> supplementation was shown to be of benefit with an acceptable safety profile (17, 18, 39). Unfortunately, mechanistic data is lacking and there has been a minimal number of studies evaluating CoQ therapy for neonatal cardiomyopathy (19). Thus, the newborn *Fmr1* KO mouse model will likely help to provide mechanistic insights in future work given the putative role of pathological opening of the mPTP in myocardial ischemia-reperfusion injury and cardiomyopathies and the association of CoQ deficiency with heart failure (4, 9, 10).

Open probability of the mPTP has been reported previously in the neonatal murine heart and closure of the pore with agents, such as CsA and NIM811, was shown to increase the mitochondrial membrane potential and enhance cardiac function within the first five days of life (2). Although we found open probability of the mPTP in wild-type cardiomyocytes on P10, closed probability of the pore within the *Fmr1* KO did not translate into an effect on absolute mitochondrial respiration or cardiac performance. This difference may relate to the developmental stage of the mice. In the current study, we evaluated 10 day old mice while prior investigation assessed mice on P5 (2). Thus, it is possible that cardiomyocyte

mitochondria may be naturally transitioning to a mature phenotype on P10 and the pore may be relatively less open in the developing heart at this age compared to the first few postnatal days of life. This may explain the absence of physiological consequences of a prematurely closed mPTP in *Fmr1* KO mice at this age and the lack of a cardiac phenotype in Fragile X Syndrome. Importantly, the mice assessed in this work were healthy and non-stressed. Therefore, it will be critical to assess how *Fmr1* KO cardiomyocytes and mitochondria respond to insult and injury. Based on our knowledge of CsA, CoQ, and the mPTP, future investigation will need to determine if the developing *Fmr1* KO heart is relatively more resilient to ischemia-reperfusion and experimental heart failure.

It is unknown how loss of FMRP causes changes in CoQ biosynthesis, stability, or turnover. FMRP is a translational repressor that binds to the mRNA of all of the known enzymes of the ubiquinone biosynthesis pathway (23). Thus, it is possible that FMRP deficiency affects CoQ biosynthesis directly. However, the FMRP-CoQ interaction is likely complex given tissue-specific differences in ubiquinone content in the *Fmr1* KO mouse. In addition, indirect effects of FMRP deficiency may exist and other mechanisms may play a role in closed or open mPTP probability. Thus, future work will be necessary and will focus on determining how loss of FMRP leads to CoQ excess in the developing heart and CoQ deficiency in the immature brain.

The data presented here establishes the newborn *Fmr1* KO mouse as a new and unique model of CoQ excess and a closed mPTP in the developing heart. We are hopeful that this model will be useful as an investigative tool to aid us in delineating the roles of ubiquinone and the pore in cardiac maturation and in the manifestation of neonatal heart failure. Greater knowledge could result in the development of novel targeted therapeutic agents aimed at treating or preventing heart failure in infants. Thus, the *Fmr1* KO mouse could be an important model to advance our understanding of fundamental cardiac developmental biology and help us gain insight into why the neonatal heart is uniquely vulnerable to injury.

## Acknowledgments

Supported by NIH/NINDS R01NS112706 (R.J.L.)

## References

1. Hsu DT, Pearson GD. Heart failure in children: part I: history, etiology, and pathophysiology. *Circ Heart Fail* 2009;2:63–70. [PubMed: 19808316]
2. Lingan J, Alanzalon RE, Porter GA Jr. Preventing permeability transition pore opening increases mitochondrial maturation, myocyte differentiation and cardiac function in the neonatal mouse heart. *Pediatr Res* 2017;81:932–941. [PubMed: 28141792]
3. Soares P, et al. Neonatal dilated cardiomyopathy. *Rev Port Cardiol.* 2017;36:201–214. [PubMed: 28256370]
4. Pérez MJ, Quintanilla RA. Development or disease: duality of the mitochondrial permeability transition pore. *Dev Biol* 2017;426:1–7. [PubMed: 28457864]
5. Beutner G, Eliseev RA, Porter GA Jr. Initiation of electron transport chain activity in the embryonic heart coincides with the activation of mitochondrial complex 1 and the formation of supercomplexes. *PLoS One* 2014;9:e113330. [PubMed: 25427064]
6. Hom JR, et al. The permeability transition pore controls cardiac mitochondrial maturation and myocyte differentiation. *Dev Cell* 2011;21:469–78. [PubMed: 21920313]

7. Alavian KN, et al. An uncoupling channel within the c-subunit ring of the F1FO ATP synthase is the mitochondrial permeability transition pore. *Proc Natl Acad Sci U S A* 2014;111:10580–5. [PubMed: 24979777]
8. Javadov S, Kuznetsov A. Mitochondrial permeability transition and cell death: the role of cyclophilin d. *Front Physiol* 2013;4:76. [PubMed: 23596421]
9. Zhu H, Sun A. Programmed necrosis in heart disease: Molecular mechanisms and clinical implications. *J Mol Cell Cardiol* 2018;116:125–134. [PubMed: 29426003]
10. Goldenthal MJ. Mitochondrial involvement in myocyte death and heart failure. *Heart Fail Rev* 2016;21:137–55 [PubMed: 26886225]
11. Javadov S, Karmazyn M, Escobales N. Mitochondrial permeability transition pore opening as a promising therapeutic target in cardiac diseases. *J Pharmacol Exp Ther* 2009;330:670–678. [PubMed: 19509316]
12. Cung TT, et al. Cyclosporine before PCI in patients with acute myocardial infarction. *N Engl J Med* 2015;373:1021–31. [PubMed: 26321103]
13. Hsu DT, Pearson GD. Heart failure in children: part II: diagnosis, treatment, and future directions. *Circ Heart Fail* 2009;2:490–8. [PubMed: 19808380]
14. Sole MJ, Jeejeebhoy KN. Conditioned nutritional requirements: therapeutic relevance to heart failure. *Herz* 2002;27:174–8. [PubMed: 12025462]
15. Licitra F, Puccio H An overview of current mouse models recapitulating coenzyme q10 deficiency syndrome. *Mol Syndromol* 2014;5:180–6. [PubMed: 25126051]
16. Walter L, et al. Three classes of ubiquinone analogs regulate the mitochondrial permeability transition pore through a common site. *J Biol Chem* 2000;275:29521–7. [PubMed: 10889201]
17. Madmani ME, et al. Coenzyme Q10 for heart failure. *Cochrane Database Syst Rev* 2014;6:CD008684.
18. Mortensen SA, et al. Q-SYMBIO study investigators. The effect of coenzyme Q10 on morbidity and mortality in chronic heart failure: results from Q-SYMBIO: a randomized double-blind trial. *JACC Heart Fail* 2014;2:641–649. [PubMed: 25282031]
19. Baghavan HN and Chopra RK. Potential role of ubiquinone (coenzyme Q10) in pediatric cardiomyopathy. *Clin Nutrition*. 2005;24:331–8.
20. Hou Y, et al. Mitochondrial superoxide production negatively regulates neural progenitor proliferation and cerebral cortical development. *Stem Cells* 2012; 30:2535–47. [PubMed: 22949407]
21. Griffiths KK, et al. Inefficient Thermogenic Mitochondrial Respiration Due to Futile Proton Leak in a Mouse Model of Fragile X Syndrome. *FASEB J*. 2020; in press.
22. Verkerk AJMH, et al. Identification of a gene (FMR-1) containing a CGG repeat coincident with a breakpoint cluster region exhibiting length variation in fragile X syndrome. *Cell* 1991;65, 905–914. [PubMed: 1710175]
23. Darnell JC, et al. FMRP stalls ribosomal translocation on mRNAs linked to synaptic function and autism. *Cell*. 2011;146,247–61. [PubMed: 21784246]
24. Miyadera H, et al. Atpenins, potent and specific inhibitors of mitochondrial complex II (succinate-ubiquinone oxidoreductase). *Proc Natl Acad Sci U S A* 2003;100,473–7. [PubMed: 12515859]
25. Spinazzi M, Casarin A, Pertegato V, Salviati L, Angelini C. Assessment of mitochondrial respiratory chain enzymatic activities on tissues and cultured cells. *Nat Protoc* 2012;7,1235–46 [PubMed: 22653162]
26. Ferreiro-Barros CC, Sugawara EK, Sanches LR. Determination of a method for extraction of coenzyme Q10 in human plasma: optimization of the use of surfactants and other variables. *Einstein (Sao Paulo)* 2012;10,203–8. [PubMed: 23052456]
27. Pumphrey AM and Redfearn ER. A method for determining the concentration of ubiquinone in mitochondrial preparations. *Biochem J* 1960;76,61–4. [PubMed: 14435319]
28. Amo T and Brand MD. Were inefficient mitochondrial haplogroups selected during migrations of modern humans? A test using modular kinetic analysis of coupling in mitochondria from hybrid cell lines. *Biochem J* 2007;404,345–51. [PubMed: 17355224]

29. Fink BD, et al. UCP2-dependent proton leak in isolated mammalian mitochondria. *J Biol Chem.* 2002;277,3918–25. [PubMed: 11723122]
30. Cardoso S, Santos MS, Moreno A, Moreira PI. UCP2 and ANT differently modulate proton-leak in brain mitochondria of long-term hyperglycemic and recurrent hypoglycemic rats. *J Bioenerg Biomembr* 2013;45,397–407. [PubMed: 23504111]
31. Hansson MJ, et al. Powerful cyclosporin inhibition of calcium-induced permeability transition in brain mitochondria. *Brain Res.* 2003;960,99–111. [PubMed: 12505662]
32. Caine C, et al. A pathogenic S250F missense mutation results in a mouse model of mild aromatic l-amino acid decarboxylase (AADC) deficiency. *Hum Mol Genet* 2017;26:4406–4415. [PubMed: 28973165]
33. Singh K, Gaur P, Prasad S. Fragile x mental retardation (Fmr-1) gene expression is down regulated in brain of mice during aging. *Mol Biol Rep* 2007;34,173–81. [PubMed: 17136426]
34. Loeperke AW, McCann JC, Kurth CD, McAuliffe JJ. The physiologic effects of isoflurane anesthesia in neonatal mice. *Anesth Analg.* 2006;102:75–80. [PubMed: 16368807]
35. Green DR and Kroemer G. The pathophysiology of mitochondrial cell death. *Science.* 2004;305,626–9. [PubMed: 15286356]
36. Brand MD and Nicholls DG. Assessing mitochondrial dysfunction in cells. *Biochem J.* 2011;435,297–312. [PubMed: 21726199]
37. Rossow HA, Acetoz G, Champagne J, Ramsey JJ. Measuring Liver Mitochondrial Oxygen Consumption and Proton Leak Kinetics to Estimate Mitochondrial Respiration in Holstein Dairy Cattle. *J Vis Exp.* 2018; 141:e58387.
38. Zhang Y, Appelkvist EL, Kristensson K, Dallner G. The lipid compositions of different regions of rat brain during development and aging. *Neurobiol Aging.* 1996;17:869–75. [PubMed: 9363798]
39. Sharma A, Fonarow GC, Butler J, Ezekowitz JA, Felker M. Coenzyme Q10 and Heart Failure A State-of-the-Art Review. *Circ Heart Fail.* 2016;9:e002639. [PubMed: 27012265]
40. Brea-Calvo G, et al. COQ4 Mutations Cause a Broad Spectrum of Mitochondrial Disorders Associated with CoQ10 Deficiency. *The American Journal of Human Genetics* 2015;96:309–17. [PubMed: 25658047]

**Impact:**

- Key message of article: Ubiquinone is in excess and the mPTP is closed in the developing FXS heart
- What is added to existing literature: Strengthens evidence of open mPTP probability in the normally developing postnatal murine heart and provides new evidence for premature closure of the mPTP in *Fmr1* mutants
- What is the impact: Establishes a novel model of excess CoQ and a closed pore in the developing heart. Such a model will be a valuable tool used to better understand the role of ubiquinone and the mPTP in the neonatal heart in health and disease

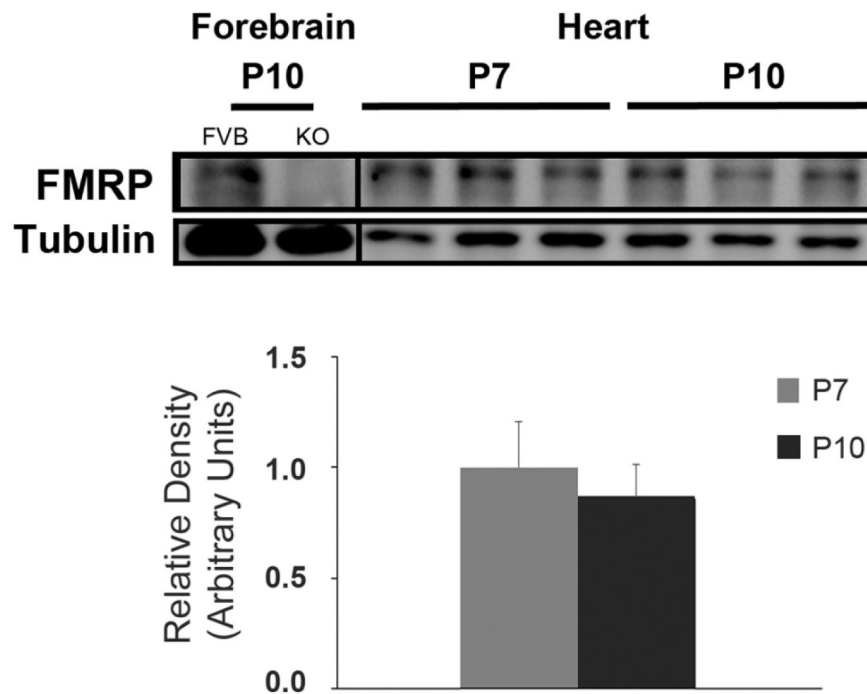


**Figure 1. Wild-type Fragile X Mental Retardation Protein (FMRP) Expression in the Developing Heart.**

Immunoblot of FMRP in cardiac ventricles is depicted. FVB mice were assessed on postnatal days 7 (P7) and P10 (n = 3 mice per time point). Densities were normalized to the tubulin loading control. Graphical representation of relative densities is shown. Normalized values from P7 FVB mouse heart were arbitrarily set to equal 1. Forebrain homogenate from P10 FVB and *Fmr1* KO mice served as positive and negative controls, respectively. As expected, no FMRP was detected in forebrain of a P10 *Fmr1* KO mouse. Values are expressed as means  $\pm$  SD. *P* = nonsignificant.

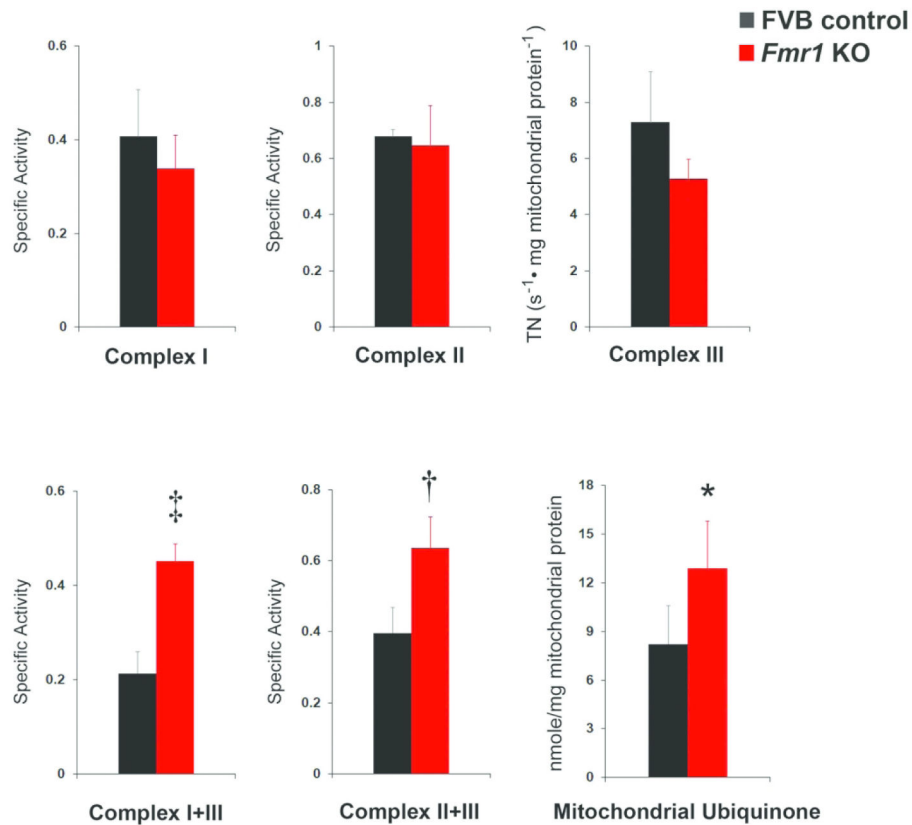


**Figure 2. Ubiquinone is in Excess in *Fmr1* KO Cardiomyocyte Mitochondria.**

The specific activities of electron transport chain Complexes I and II are depicted. First order rate constants were determined for Complex III and expressed as turnover number (TN). The CoQ pool was assessed indirectly by measuring the linked kinetic activities of Complex I+III and Complex II+III. Ubiquinone content was measured directly in cardiomyocyte mitochondria via spectrophotometry. Values are expressed as means  $\pm$  SD.  $n = 5-7$  animals per group.  $P$  values were calculated by Student's  $t$  test. \* $P < 0.05$ , † $P < 0.01$ , ‡ $P < 0.001$ .

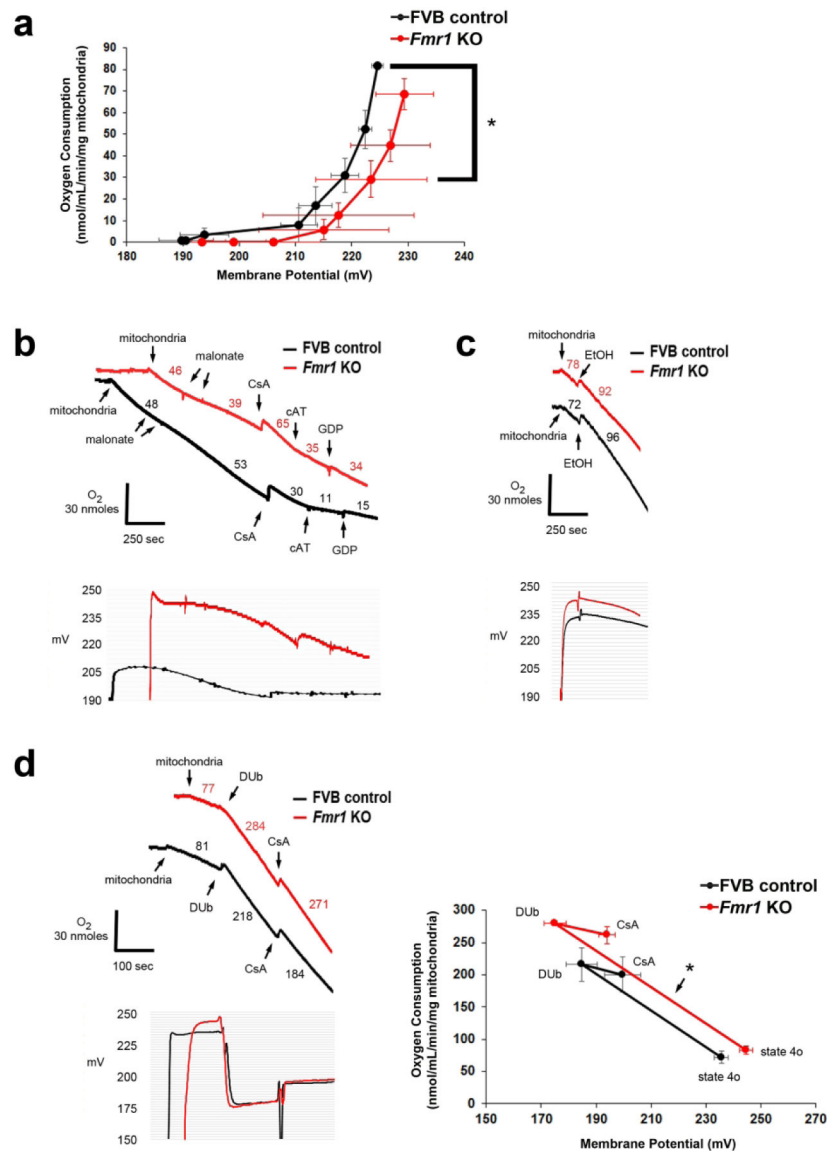


**Figure 3. Proton Leak Kinetics and Source of Leak in Developing Cardiomyocyte Mitochondria.** (a) Proton Leak Kinetics. Rates of oxygen consumption using succinate as a substrate were measured over a range of mitochondrial membrane potentials. State 4 was induced with oligomycin (data point with highest membrane potential) and respiration was titrated with serial additions of malonate.  $n = 3$  animals per group. Values are expressed as means  $\pm$  SEM.  $P$  values for the rate of oxygen consumption at the highest common membrane potential were calculated by Student's  $t$  test.  $*P < 0.05$ . (b-d) Oligomycin-induced state 4 (state 4<sub>o</sub>) was initiated using succinate as a substrate. Representative tracings of oxygen consumption (above) with simultaneous mitochondrial membrane potential measurement (below) are depicted. Numbers indicate rates of oxygen consumption ( $\text{nmol} \cdot \text{mL}^{-1} \cdot \text{min}^{-1} \cdot \text{mg}$  mitochondrial protein<sup>-1</sup>). (b) Source of proton leak. Titrations of malonate were used to induce voltage-gated proton leak. Cyclosporine A (CsA), carboxyatractyloside (cAT), and guanosine diphosphate (GDP) were added to specifically inhibit proton leak via the

mitochondrial permeability transition pore (mPTP), the adenine nucleotide translocase (ANT) and uncoupling proteins (UCPs), respectively (30, 31). Experiments were repeated in 8–10 animals per group. (c) Effect of ethanol solvent (EtOH). Experiments were repeated in 2–3 animals per group. (d) Decylubiquinone (DUb) was added to antagonize endogenous CoQ. Representative tracings are shown on the left. Graphical depiction of oxygen consumption relative to membrane potential following the addition of DUb and CsA is shown on the right.  $n = 3$  animals per group. Values are expressed as means  $\pm$  SD.  $P$  values for change in the rate of oxygen consumption and change membrane potential were calculated by Student's  $t$  test. \* $P < 0.05$ .

Author Manuscript

Author Manuscript

Author Manuscript

Author Manuscript

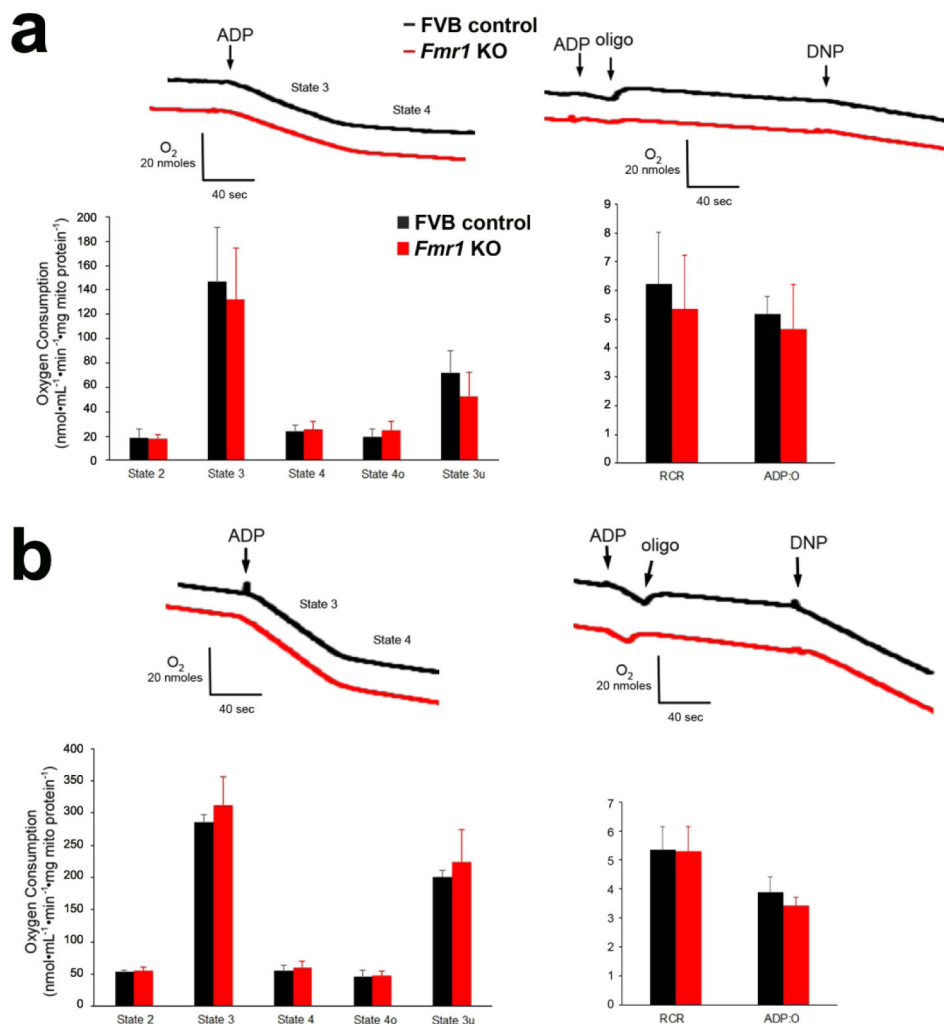


**Figure 4. Oxygen Consumption in *Fmr1* KO and FVB Control Mitochondria.**

Representative tracings for (a) Complex I-dependent oxygen consumption using glutamate/malate (n = 5 controls, 7 KOs) and (b) Complex II-dependent oxygen consumption using succinate (n = 5 controls, 8 KOs) are depicted. Graphical representation of state 2 respiration (following addition of substrate), state 3 respiration (following addition of adenosine diphosphate (ADP)), state 4 respiration, uncoupled state 3 respiration (state 3u; following addition of dinitrophenol (DNP)), and oligomycin-induced state 4 (state 4o) are shown below the respective tracings. Graphical depiction of respiratory control ratios (RCR) and adenosine diphosphate-to-oxygen ratios (ADP:O) are also shown. Values are expressed as means  $\pm$  SD. *P* values were nonsignificant.

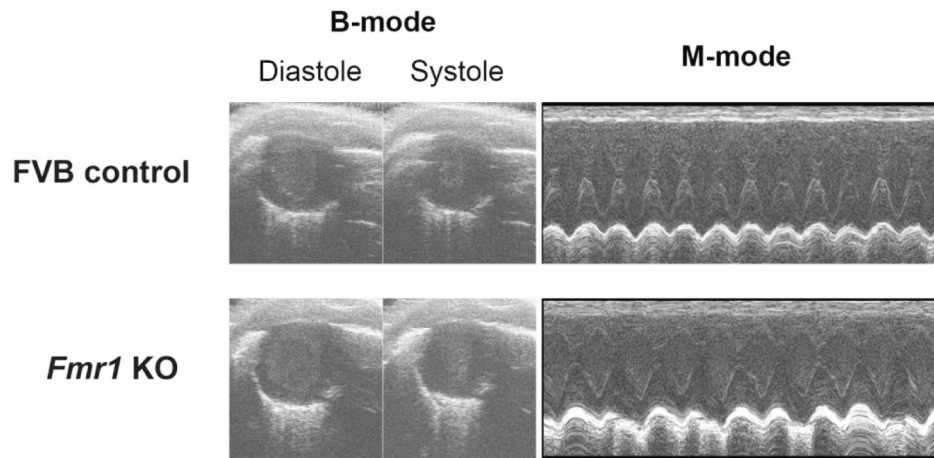


**Figure 5. Echocardiographic Images in *Fmr1* KO Mice and FVB Controls.**

Parasternal short axis images were obtained in B-mode and M-mode to quantify end-diastolic left ventricular dimension and end-systolic left ventricular dimension.

Representative images are depicted for both strains.

**Table.**Cardiac Function in *Fmr1* KO Mice and FVB Controls.

Parameter	Strain	
	FVB	<i>Fmr1</i> KO
Heart rate, beats/min	375 ± 45	378 ± 37
End-diastolic left ventricular dimension, mm	2.1 ± 0.1	2.2 ± 0.1
End-systolic left ventricular dimension, mm	1.3 ± 0.1	1.4 ± 0.1
Fractional shortening, %	38.9 ± 1.2	36.1 ± 3.2

Values are expressed as means ± SD. n = 5 mice per group. *P* values are nonsignificant.

Author Manuscript

Author Manuscript

Author Manuscript

Author Manuscript